IEEE Access
Multidisciplinary | Rapid Review | Open Access Journal

Received December 11, 2021, accepted February 5, 2022, date of publication February 11, 2022, date of current version February 18, 2022.

Digital Object Identifier 10.1109/ACCESS.2022.3151100

Degradation Observations of Protective Coatings: An Improved Version of Coating Impedance Detector

HUAN-CHENG LIAO[1], ZONG-HAN CAI[1], HUNG-HSUN CHEN[1], CHENG-HSIEN CHUNG[2], I-CHUNG CHENG[3], AND YUEH-LIEN LEE[1], (Member, IEEE)

[1]Department of Engineering Science and Ocean Engineering, National Taiwan University, Taipei 10617, Taiwan
[2]Ship and Ocean Industries Research and Development Center (SOIC), Taipei 100210, Taiwan
[3]Department of Mechanical Engineering, National Taiwan University, Taipei 10617, Taiwan

Corresponding author: Yueh-Lien Lee (yuehlien@ntu.edu.tw)

This work was supported in part by the Ship and Ocean Industries Research and Development Center under Grant 110-04B.

ABSTRACT This study proposes coating impedance detector 3.0 (CID 3.0), an improved version of our previously developed CID 2.0. The new circuit design in CID 3.0 has lower power consumption because it has fewer components, and it affords better accuracy through the modification of the analog part of CID 2.0 and the use of oversampling. This approach successfully afforded CID 3.0 with higher measurement stability for evaluating a high-performance coating with impedance values exceeding 10^9 Ω. Furthermore, CID 3.0 could detect impedance decreases associated with coating delamination when the coating suffers an attack.

INDEX TERMS Coating degradation, corrosion monitor, field-programmable gate array, oversampling, electrochemical impedance spectroscopy.

I. INTRODUCTION

Among many corrosion prevention methods, such as sacrificial anode and impressed current cathodic protection, protective organic coatings are considered the most low-cost, direct, and effective solution for offshore wind turbines. Such coatings, in a manner similar to those on ships and buildings, can provide a physical barrier to protect offshore wind turbines from corrosive environments. However, the coating health gradually deteriorates with time. In other words, coatings cannot provide permanent protection to a substrate, and they must be periodically inspected and maintained to maximize their lifetime and ensure their function. Offshore environments are extremely corrosive owing to the presence of numerous corrosion factors, including chloride ions in seawater and ultraviolet rays in sunlight. The wet–dry cycling conditions at the splash zone are considered another major factor causing the degradation of coatings. Therefore, the health of coatings applied on steel structures should be evaluated periodically to prevent corrosion failures in offshore wind towers.

As an alternative to the well-known traditional testing methods (e.g., the salt spray test [1] and QUV accelerated weathering test [2]), in recent years, many studies have investigated nondestructive testing (NDT) and strategies for evaluating the properties of a coating—specifically, acoustic emission [3], ultrasonic [4], eddy current [5]–[7], infrared thermography [8]–[10], optical [11]–[14], electrical [15], [16], and electrochemical testing [17]–[29] methods. All these methods have their own advantages, however, each of them also has its particular limitations. For example, a smooth or polished surface is required for ultrasonic and eddy current techniques; the electrical resistance (ER) sensor technique is more suitable for measuring uniform corrosion than localized corrosion; the infrared thermography technique has disadvantages such as a time-consuming process and the need for relatively expensive microwave equipment [8]; and the embedding of optical fibers runs the risk of decreased coating protectiveness through decreased adhesion or increased defect formation [30]. More importantly, these aforementioned methods are incapable of characterizing and monitoring the early degradation of organic coatings or being applied in field monitoring.

Electrochemical techniques have been successfully used in corrosion and coating studies over the past several decades. Among these techniques, electrochemical impedance spectroscopy (EIS) is the most popular for investigating the protective properties of coatings systems on metals. EIS is

The associate editor coordinating the review of this manuscript and approving it for publication was Leonel Sousa.

a nondestructive method that can be used to evaluate the health of organic coatings. The advantages of EIS are its precise, stable, and reliable performance and ability to provide complete and detailed impedance information regarding coatings. This information can be used to evaluate the health of coatings and accordingly schedule early maintenance. The disadvantages of EIS include its high cost; bulky hardware; and requirement of a low-disturbance environment, steady power supply, and other additional equipment; these disadvantages limit its usability for in situ measurements. As a result, many researchers have aimed to simplify the EIS experimental setup and accordingly proposed simplified EIS-based monitoring systems [18]–[29]. For example, Sebar *et al.* recently formulated a portable low-cost device for performing EIS measurements [29]. This instrument can measure the impedance in the frequency range from 0.01 Hz to 50 kHz. Further, the system uncertainty is less than 5% for an impedance of up to 50 kΩ. Unfortunately, they did not test the instrument's accuracy on coated samples; they only used a known capacitor, resistor, and metallic substrate. In addition, the measurement of a wide frequency range (0.1 Hz to 10k Hz) to obtain the full impedance spectra may limit the possibility of further reducing the measurement time. In 1999, Davis *et al.* proposed an EIS-based in situ corrosion sensor called a coating health monitor (CHM) to detect coating defects and to monitor the coating degradation in Army ground vehicles. This simplified impedance measuring system was designed to take three single-frequency electrochemical impedance measurements at 0.2, 0.5, and 0.9 Hz, respectively. The CHM results indicated that the EIS measurements at three frequencies agreed well with those obtained using a commercial Gamry potentiostat (Warminster, PA, USA) for a resistor–capacitor circuit and a coated specimen [18]. Although the CHM is a battery-powered, wireless microsensor system with EIS functionality, it may not be suitable for onsite monitoring because of its high cost and limited performance (e.g., CHM cannot measure a coating with an impedance above 5×10^8 Ω-cm^2) [24]. Lee *et al.* proposed a prototype miniaturized impedance measurement instrument and demonstrated that it can provide a quick estimate of the protective capacity of coatings [24].

In our previous study, an Altera DE0-Nano field-programmable gate array (FPGA) was employed for developing an innovative, compact, and portable second-generation coating impedance detector (CID 2.0) [25]. CID 2.0 consists of an FPGA and a custom printed circuit board (PCB) that mainly performs the voltage division used to calculate the impedance of coatings. Fig. 1 displays the measurement setup of CID 2.0. An oscilloscope and signal generator were successfully integrated in CID 2.0 by using the FPGA. CID 2.0 has dimensions of only $5 \times 9 \times 0.16$ cm^3, making it considerably smaller than the first-generation CID and a conventional potentiostat system. Previous experimental results indicated that the FPGA-based CID 2.0 can reliably measure impedance values of 10^6 to 10^{10} Ω-cm^2.

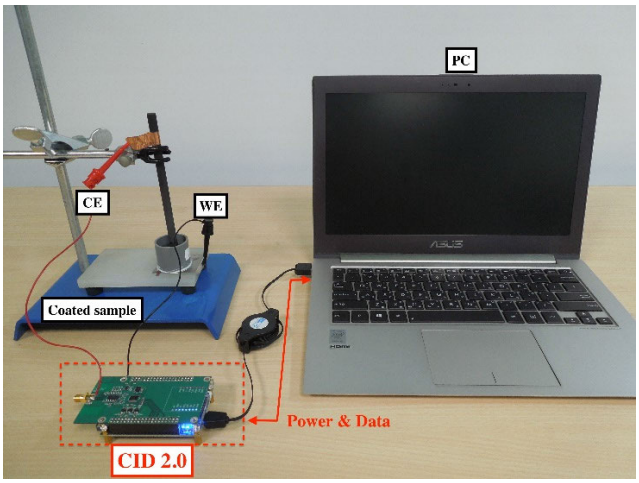

FIGURE 1. Measurement configuration of CID 2.0 [24].

Although CID 2.0 can detect variations in the coating impedance value in the range of 10^5 to 10^9 Ω (as raw measurements without normalization by the subject area of 7.8 cm^2), its feasibility and accuracy for measuring a thick and high-performance coating having impedance exceeding 10^9 Ω remain a serious concern. Fig. 2 indicates that although the average impedance value measured by CID 2.0 (4.51×10^9 Ω) is close to that obtained using a commercial potentiostat (2.78×10^9 Ω), CID 2.0 measurements had a standard deviation of up to 3.01×10^9 Ω, suggesting that these measurements could be unreliable when the raw impedance value of the examined samples exceeds 10^9 Ω. To reduce data uncertainty and increase the measurement reliability when the examined coatings have high impedance values, as is the case with the commercial paints applied within the offshore wind energy industry, this study proposes CID 3.0, a revised version of CID 2.0. By modifying the analog part of CID 2.0 and using oversampling, the overall noise is reduced to a lower level with CID 3.0. This feature is expected to allow CID 3.0 to achieve a much higher accuracy and working range compared with CID 2.0. More importantly, these notable system performance improvements achieved using the newly designed detector incur no additional cost and require no substantial change in size, suggesting that CID 3.0 would be more suitable than CID 2.0 for practical applications in the health monitoring of extremely robust coatings in the field. In this study, the impedance of commercial coated samples measured using CID 3.0 was recertified and compared with that of samples measured using the conventional potentiostat. Continuous monitoring experiments were also conducted to demonstrate the efficiency of CID 3.0 in monitoring the coating degradation.

II. SYSTEM DESIGN

The previous version of our instrument uses two unity-gain buffer circuits and two analog-to-digital converters (ADCs) to measure the input voltage signal and the impedance-divided voltage signal [Fig. 3(a)]. The goal was to reduce

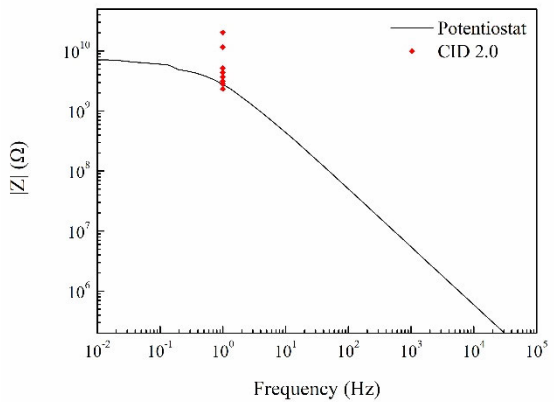

FIGURE 2. Comparison of results obtained using CID 2.0 and conventional potentiostat for a high-performance commercial coating.

the need for calibration without using any external resistors other than the reference resistor. However, the ADCs have internal preamplifiers, and mismatches exist between the two ADCs. Consequently, calibration would still be required to improve measurement accuracy. In this study, an improved version with higher measurement accuracy was implemented. Because calibration is unavoidable if one wishes to achieve high accuracy, the measurement of the input signal is removed; thus, only one operational amplifier and one ADC are required, resulting in a 50% lower power consumption. Moreover, the gain can now be provided by the operational amplifier to improve the signal-to-noise ratio (SNR) of the signal going into the ADC. Therefore, the new circuit has lower power consumption with fewer components and better accuracy through the improved SNR and calibration compared with the previous implementation.

Fig. 3(b) presents the block diagram of CID 3.0. The FPGA generates a continuous 10-mV sinusoidal signal with a frequency of 0.5 Hz (V_1 in Fig. 3(b)). According to the Friis formula, when the overall gain of a cascade of stages remains the same, the overall noise figure is lower if the first stage's gain is higher. CID 2.0 used two unity buffers at the first stage of the system. In CID 3.0, these unity buffers are replaced with a noninverting amplifier to reduce the overall noise and simultaneously ensure v1 is unaffected by the loading effect.

To further reduce noise, the sampling rate, $f_{sampling}$, of the ADC was increased. When the sampling rate is higher, the spreading interval of noise increases. Therefore, the quantization noise is divided by the oversampling ratio (OSR). The relationship between OSR and SNR can be expressed as

$$\mathrm{OSR} = \frac{f_{sampling}}{2 \times f_{signal}} \tag{1}$$

$$\mathrm{SNR(dB)} = 1.76\mathrm{dB} + 6.02\mathrm{N} + 10\log(\mathrm{OSR}) \tag{2}$$

where f_{signal} is 0.5 Hz in CID 3.0. Based on (2), by increasing $f_{sampling}$, signals are less affected by noise in CID 3.0 than in CID 2.0. According to Kirchoff's law, V_2 can be expressed as

$$V_2(0.5\mathrm{Hz}) = V_s(0.5\mathrm{Hz}) \times \mathrm{G} \times \frac{Z_{dut}}{R_{ref} + Z_{dut}} \tag{3}$$

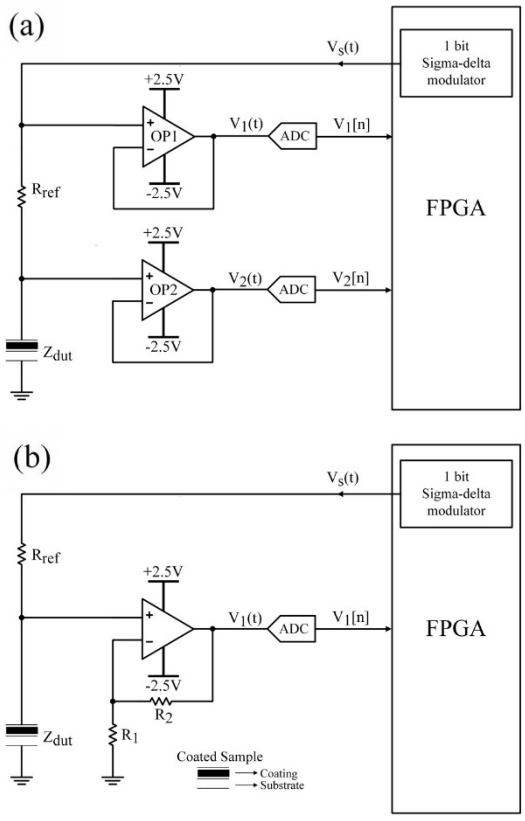

FIGURE 3. Block diagram of (a) CID 2.0 and (b) CID 3.0.

where V_2 (0.5 Hz) and V_S (0.5 Hz) are the Fourier transforms of $V_2(t)$ and $V_s(t)$, respectively, at 0.5 Hz, and G is the noninverting amplifier's gain, which can be calculated as

$$\mathrm{G} = \frac{R1 + R2}{R1} \tag{4}$$

When the coated sample is not connected to the circuit, the circuit is open and Z_{dut} in (3) approaches infinity. Therefore, V_2 can be expressed as

$$V_2\ (0.5\mathrm{Hz})\ |_{Z_{dut} \to \infty} = V_s(0.5\mathrm{Hz}) \times \mathrm{G} \tag{5}$$

Finally, the relationship between Z_{dut} and R_{ref} can be expressed as

$$\frac{Z_{dut}}{R_{ref} + Z_{dut}} = \frac{V_2(0.5\mathrm{Hz})}{V_2\ (0.5\mathrm{Hz})\ |_{Z_{dut} \to \infty}} \tag{6}$$

Therefore, Z_{dut} can be found by solving (6). Notably, R_1 and R_2 are not variables in (6). Therefore, their precise values need not be known to calculate Z_{dut}. The resistors R_1 and R_2 solely provide gain to the input signal and thus improve the noise performance.

III. EXPERIMENTAL PROCEDURE

Seven ideal resistors with resistances ranging from 10^4 to 10^{10} Ω and various coating system samples with impedance values (raw measurement) exceeding 10^9 Ω, including aluminum substrates with a 75-μm-thick epoxy coating system

and two 450- and 550-μm-thick high-performance commercial coated steels, were prepared to verify the accuracy and performance range of the proposed device. For comparison, the impedance was also measured using a conventional potentiostat (Ref 600, Gamry Instruments, Pennsylvania, USA). A potentiostat with a standard three-electrode setup was used; it comprised the coated sample as the working electrode, a saturated calomel reference electrode, and a graphite rod as the counter electrode. CID 3.0 was used with a simplified two-electrode setup that is more suitable for installation in the field. The exposed surface area of the coated sample was 0.78 cm^2, and the working electrolyte was a 3.5 wt% NaCl solution. To evaluate the monitoring function, a knife was used to scratch the coated samples (length of the scratch: 5 mm) to create an artificial defect in both lab and field EIS monitoring tests. After the artificial defect was produced, the impedance value of the damaged sample was measured using a potentiostat and CID 3.0.

IV. RESULTS AND DATA ANALYSIS

A. HARDWARE IMPROVEMENT

To estimate the accuracy of the CID 3.0 measurements, the impedance values of seven ideal resistors with resistances of 10^4 to 10^{10} Ω were measured using CID 3.0 and a commercial volt-ohm-milliammeter (VOM). Table 1 presents a summary of the measurement results. The impedance values of the seven ideal resistors as obtained using CID 3.0 were 9.78 kΩ, 99.4 kΩ, 0.992 MΩ, 9.91 MΩ, 101.18 MΩ, 1.072 GΩ, and 9.07 GΩ, respectively; these are similar to the values measured by VOM. This finding indicates favorable accuracy because the error of the impedance values between CID 3.0 and VOM is within 3%.

Fig. 4 illustrates Bode magnitude plots of three coated samples as measured using a potentiostat; the green points in the three figures indicate the average impedance value of five raw measurements at 0.5 Hz as obtained using CID 3.0. In Fig. 4(a), the $|Z|_{0.5Hz}$ value of the 75-μm-thick epoxy-coated Al substrate as measured using the potentiostat was 3.03×10^8 Ω. The average of five $|Z|_{0.5Hz}$ values obtained using CID 3.0 for the same coating sample was 3.64×10^8 Ω with a standard deviation of 5.57×10^6 Ω. Moreover, in Fig. 4(b), the $|Z|_{0.5Hz}$ value of the 450-μm-thick commercial coated steel substrate as measured using the potentiostat was 0.98×10^9 Ω. The average of five $|Z|_{0.5Hz}$ values obtained using CID 3.0 for the same coating sample was 1.11×10^9 Ω with a standard deviation of 1.69×10^7 Ω. Notably, for the 550-μm-thick commercial coated steel substrate (Fig. 4(c)), the $|Z|_{0.5Hz}$ value of the coated sample as measured using the potentiostat was as high as 1.37×10^{10} Ω, and the average of five $|Z|_{0.5Hz}$ values obtained using CID 3.0 for the same coating sample was 1.35×10^{10} Ω with a standard deviation of 2.02×10^9 Ω. The measurement results obtained using CID 3.0 and the potentiostat for the three coated samples were in agreement with each other. Overall, the performance of CID 3.0 was comparable to that of CID 2.0. Moreover, the accuracy and stability of CID 3.0 for estimating the impedance values of high-quality coatings were higher than those of CID 2.0.

TABLE 1. Measurement data of commercial VOM and CID 3.0.

Resistor (Ω)	VOM	CID 3.0	Standard deviation	Error (%)
10k	10.01k	9.78k	3.3k	2.30
100k	99.7k	99.4k	1.15k	0.29
1M	0.990M	0.992M	12.4k	0.19
10M	9.87M	9.91M	47.6k	0.45
100M	101.20M	101.18M	0.23M	0.02
1G	1.075G	1.072G	4.75M	0.28
10G	9.10G	9.07G	0.43G	0.35

TABLE 2. Measurement data of long-term corrosion monitoring.

Sample (Ω)	Potentiostat	CID 3.0
1 h	1.33×10^{10}	1.35×10^{10}
24 h	1.14×10^{10}	1.12×10^{10}
36 h	1.13×10^{10}	1.09×10^{10}
48h(with scratch)	8.55×10^{9}	7.74×10^{9}
60h(with scratch)	5.31×10^{9}	4.56×10^{9}

B. MONITORING DEGRADATION OF PROTECTIVE COATINGS

After the successful improvement of the CID measurement accuracy for measuring the high-performance coating, the feasibility of using CID 3.0 to periodically detect the impedance values of coatings required reconfirmation to ensure coating degradation could be detected. Fig. 5 presents the Bode plots (solid and dashed colored line) measured using the potentiostat and single-frequency impedance value (colored points) measured using CID 3.0 after immersion at various durations. First, in the Bode plots obtained using potentiostat measurements, the epoxy coating exhibited almost an inclined line with high impedance value (exceeding 10^{10} Ω-cm^2 at the lowest frequency of 10^{-2} Hz) at the beginning of the test, indicating its excellent barrier property. Subsequently, an artificial scratch was introduced on the coating to initiate the degradation of the protective coating 48 h after immersion; subsequently, the impedance value of the damaged coating was measured (dashed lines in Fig. 5). The substantial decrease in low-frequency impedance values for a damaged coating sample after 60 h of immersion clearly indicated that the loss of barrier properties occurred because of the penetration of water and electrolyte through the pores and defects of the coating [31]. Similar to the $|Z|_{0.5Hz}$ value measured using the potentiostat, the $|Z|_{0.5Hz}$ value abruptly decreased immediately in the measurement result obtained using CID 3.0, suggesting that CID 3.0 can sensitively measure changes in the coating impedance value as well. Table 2 summarizes the measurement data of $|Z|_{0.5Hz}$ values obtained using CID 3.0 and the potentiostat.

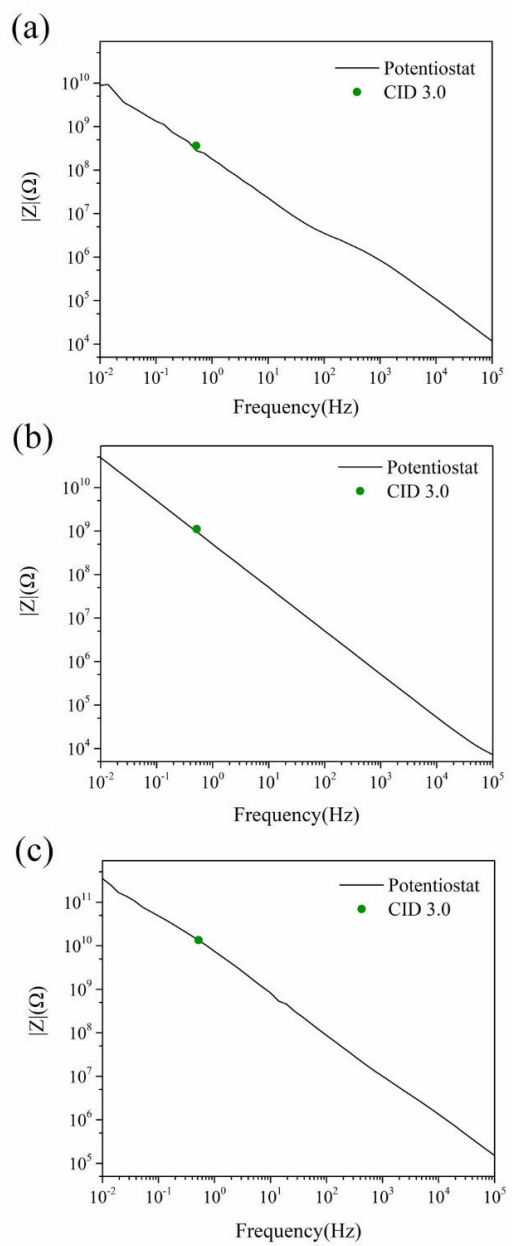

FIGURE 4. Comparison of results obtained using CID 3.0 and conventional potentiostat for (a) 75-μm-thick epoxy-coated Al substrate, (b) 450-μm-thick commercial coated steel substrate, and (c) 550-μm-thick commercial coated steel substrate.

TABLE 3. Measurement data of long-term corrosion monitoring in field environment.

Sample (Ω)	Potentiostat	CID 3.0
1 h	1.00×10^{10}	9.62×10^{10}
24 h	1.02×10^{10}	9.73×10^{10}
48 h	8.83×10^{10}	8.26×10^{10}
49h(with scratch)	5.82×10^{9}	5.62×10^{9}
72h(with scratch)	4.83×10^{9}	4.83×10^{9}

C. FIELD TESTING OF PROTECTIVE COATINGS

In addition to the corrosion monitoring results obtained under laboratory conditions, the feasibility of using CID 3.0 to detect changes in the impedance of coatings under field conditions was also evaluated in this study. The coated samples were prepared and positioned with a tilt angle of 30° under outdoor atmospheric conditions, following which they underwent dry and rainy periods during these evaluations. Fig. 6 presents the Bode plots measured using the potentiostat (solid and dashed colored line) and single-frequency impedance value (colored points) measured using CID 3.0 after exposure at various durations. The consistent Bode plots and stable impedance results obtained using potentiostat measurements and CID 3.0 both indicated that the coatings retained their qualities as an excellent barrier after the first 48 h of exposure. After an artificial scratch was made on the coating 48 h after exposure, the low-frequency impedance values of the damaged coating sample after 1 (the 49th hour) and 24 (the 72th hour) h of exposure substantially decreased, indicating that the coating loses its protection barrier as a result of the scratch. Similar to the $|Z|_{0.5Hz}$ value measured using the potentiostat, the $|Z|_{0.5Hz}$ value abruptly decreased in the measurement result obtained using CID 3.0. This experiment demonstrated the feasibility of CID 3.0 for

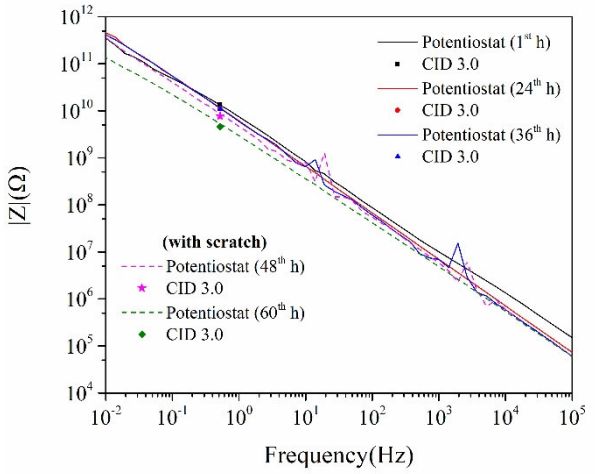

FIGURE 5. Results of long-term corrosion monitoring in lab environment.

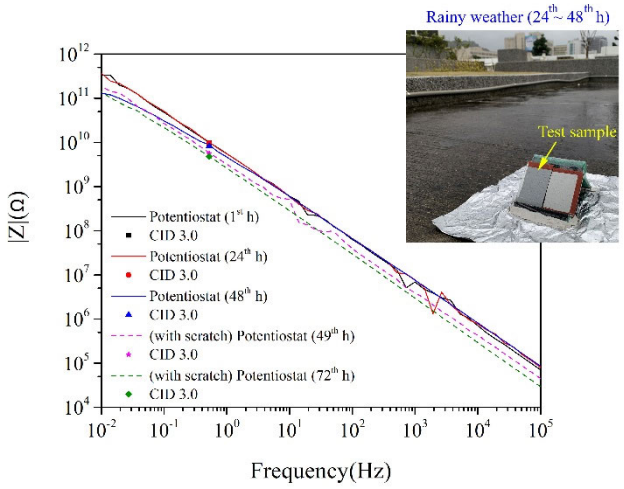

FIGURE 6. Results of long-term corrosion monitoring in field environment.

use in the field. Table 3 summarizes the measurement data of $|Z|_{0.5Hz}$ values obtained using CID 3.0 and the potentiostat in the field environment. Overall, although CID 3.0 could not provide a detailed performance assessment of coatings and provide kinetic information regarding the corrosion process, it is highly useful to engineers in determining whether coating maintenance should be scheduled through the monitoring of changes in the coating impedance values.

V. CONCLUSION

A practical and reliable CID 3.0, an improved version of CID 2.0, was proposed and characterized in this study for the rapid detection of coating degradation. The consistency between the impedance values measured using CID 3.0 and the commercial VOM for a given resistor in the range of 10^3 to 10^9 Ω demonstrated the reliability of CID 3.0. More importantly, compared with CID 2.0, CID 3.0 exhibited a higher estimated accuracy when raw measurements were conducted on the high-performance coated sample with impedance values exceeding 10^9 Ω, thus extending the applicability of CID 3.0 to diverse commercial coating systems. The corrosion monitoring measurement results also demonstrate that CID 3.0 can detect changes in the impedance value of coatings when they degrade in a corrosive environment. A CID with wireless communication function (CID 4.0) will be studied in the future.

ACKNOWLEDGMENT

The authors would like to thank Dr. Jau-Horng Chen from National Taiwan University and Dr. Cheng-Hsien Chung from the Ship and Ocean Industries Research and Development Center (SOIC) for the technical assistance and valuable advice.

REFERENCES

[1] ASTM, *Standard Practice for Operating Salt Spray (Fog) Apparatus*, Standard ASTM B117-19, 2019.

[2] ASTM, *Standard Practice for Operating Fluorescent Ultraviolet (UV) Lamp Apparatus for Exposure of Nonmetallic Materials*, Standard ASTM 154, pp. 1–12, 2016.

[3] F. Zhou, Y. Wang, M. Liu, C. Deng, X. Zhang, and Y. Wang, "Acoustic emission monitoring of the tensile behavior of a HVOF-sprayed NiCoCrAlYCe coating," *Appl. Surf. Sci.*, vol. 504, Feb. 2020, Art. no. 144400.

[4] H. Liu, L. Zhang, H. F. Liu, S. Chen, S. Wang, Z. Zheng, and K. Yao, "High-frequency ultrasonic methods for determining corrosion layer thickness of hollow metallic components," *Ultrasonics*, vol. 89, pp. 166–172, Sep. 2018.

[5] M. Grosso, C. J. Pacheco, M. P. Arenas, A. H. M. Lima, I. C. P. Margarit-Mattos, S. D. Soares, and G. R. Pereira, "Eddy current and inspection of coatings for storage tanks," *J. Mater. Res. Technol.*, vol. 7, no. 3, pp. 356–360, Jul. 2018.

[6] D. He, M. Kusano, and M. Watanabe, "Detecting the defects of warm-sprayed Ti-6Al-4 V coating using eddy current testing method," *NDT E Int.*, vol. 125, Jan. 2022, Art. no. 102565.

[7] L. Yong, Z. Chen, Y. Mao, and Q. Yong, "Quantitative evaluation of thermal barrier coating based on eddy current technique," *NDT E Int.*, vol. 50, pp. 29–35, Sep. 2012.

[8] R. Yang, Y. He, H. Zhang, and S. Huang, "Through coating imaging and nondestructive visualization evaluation of early marine corrosion using electromagnetic induction thermography," *Ocean Eng.*, vol. 147, pp. 277–288, Jan. 2018.

[9] S. Doshvarpassand, C. Wu, and X. Wang, "An overview of corrosion defect characterization using active infrared thermography," *Infr. Phys. Technol.*, vol. 96, pp. 366–389, Jan. 2019.

[10] L. Shi, Y. Long, Y. Wang, X. Chen, and Q. Zhao, "On-line detection of porosity change of high temperature blade coating for gas turbine," *Infr. Phys. Technol.*, vol. 110, Nov. 2020, Art. no. 103415.

[11] C. Guo, L. Fan, C. Wu, G. Chen, and W. Li, "Ultrasensitive LPFG corrosion sensor with Fe-C coating electroplated on a Gr/AgNW film," *Sens. Actuators B, Chem.*, vol. 283, pp. 334–342, Mar. 2019.

[12] C. Zamarreño, P. Rivero, M. Hernaez, J. Goicoechea, I. Matías, and F. Arregui, "Optical sensors for corrosion monitoring," in *Intelligent Coatings for Corrosion Control*. Amsterdam, The Netherlands: Elsevier, 2015, pp. 603–640, doi: 10.1016/B978-0-12-411467-8.00018-0.

[13] F. Deng, Y. Huang, and F. Azarmi, "Corrosion behavior evaluation of coated steel using fiber Bragg grating sensors," *Coatings*, vol. 9, no. 1, p. 55, 2019.

[14] F. Deng, Y. Huang, F. Azarmi, and Y. Wang, "Pitted corrosion detection of thermal sprayed metallic coatings using fiber Bragg grating sensors," *Coatings*, vol. 7, no. 3, p. 35, Feb. 2017.

[15] E. Diler, F. Ledan, N. LeBozec, and D. Thierry, "Real-time monitoring of the degradation of metallic and organic coatings using electrical resistance sensors," *Mater. Corrosion*, vol. 68, no. 12, pp. 1365–1376, 2017.

[16] J. K. Sell, H. Enser, B. Jakoby, M. Schatzl-Linder, B. Strauss, and W. Hilber, "Printed embedded transducers: Capacitive touch sensors integrated into the organic coating of metalic substrates," *IEEE Sensors J.*, vol. 16, no. 19, pp. 7101–7108, Oct. 2016.

[17] J. Latif, Z. A. Khan, and K. Stokes, "Structural monitoring system for proactive detection of corrosion and coating failure," *Sens. Actuators A, Phys.*, vol. 301, Jan. 2020, Art. no. 111693.

[18] G. D. Davis, R. C. Dunn, and R. A. Ros, "Wireless, battery-powered coating health monitor (CHM)," in *Proc. CORROSION*, 2010, pp. 1–9.

[19] S. Corbellini, M. Parvis, and S. Grassini, "Noninvasive solution for electrochemical impedance spectroscopy on metallic works of art," *IEEE Trans. Instrum. Meas.*, vol. 61, no. 5, pp. 1193–1200, May 2012.

[20] J. Jiang, X. Wang, R. Chao, Y. Ren, C. Hu, and Z. Xu, "Smartphone based portable bacteria pre-concentrating microfluidic sensor and impedance sensing system," *Sens. Actuators B, Chem.*, vol. 193, pp. 653–659, Mar. 2014.

[21] E. Angelini, S. Corbellini, M. Parvis, F. Ferraris, and S. Grassini, "An arduino-based EIS with a logarithmic amplifier for corrosion monitoring," in *Proc. IEEE Int. Instrum. Meas. Technol. Conf. (I2MTC)*, May 2014, pp. 905–910.

[22] S. Grassini, S. Corbellini, E. Angelini, F. Ferraris, and M. Parvis, "Low-cost impedance spectroscopy system based on a logarithmic amplifier," *IEEE Trans. Instrum. Meas.*, vol. 64, no. 5, pp. 1110–1117, May 2015.

[23] S. Grassini, S. Corbellini, M. Parvis, E. Angelini, and F. Zucchi, "A simple arduino-based EIS system for *in situ* corrosion monitoring of metallic works of art," *Measurement*, vol. 114, pp. 508–514, Jan. 2018.

[24] Y.-T. Kuo, C.-Y. Lee, and Y.-L. Lee, "Compact coating impedance detector for fast evaluation of coating degradation," *Measurement*, vol. 124, pp. 303–308, Aug. 2018.

[25] Y. Lee, Y. Kuo, H. Chen, and Y. Hsieh, "Field-programmable gate array-based coating impedance detector for rapid evaluation of early degradation of protective coatings," *IEEE Access*, vol. 7, pp. 20472–20478, 2019.

[26] M. Grossi, C. Parolin, B. Vitali, and B. Riccò, "Electrical impedance spectroscopy (EIS) characterization of saline solutions with a low-cost portable measurement system," *Eng. Sci. Technol., Int. J.*, vol. 22, no. 1, pp. 102–108, Feb. 2019.

[27] L. E. Sebar, E. Angelini, S. Grassini, L. Iannucci, and M. Parvis, "An op amp-less electrochemical impedance spectroscopy system," in *Proc. IEEE Int. Instrum. Meas. Technol. Conf. (I2MTC)*, May 2020, pp. 1–6.

[28] Y. Matsubara, "A small yet complete framework for a potentiostat, galvanostat, and electrochemical impedance spectrometer," *J. Chem. Educ.*, vol. 98, no. 10, pp. 3362–3370, 2021.

[29] L. E. Sebar, L. Iannucci, E. Angelini, S. Grassini, and M. Parvis, "Electrochemical impedance spectroscopy system based on a teensy board," *IEEE Trans. Instrum. Meas.*, vol. 70, pp. 1–9, 2021.

[30] T. Savill and E. Jewell, "Techniques for *in situ* monitoring the performance of organic coatings and their applicability to the pre-finished steel industry: A review," *Sensors*, vol. 21, no. 19, p. 6334, Sep. 2021.

[31] Y. González-García, S. González, and R. M. Souto, "Electrochemical and structural properties of a polyurethane coating on steel substrates for corrosion protection," *Corrosion Sci.*, vol. 49, pp. 3514–3526, Sep. 2007.

HUAN-CHENG LIAO received the B.S. degree from the Department of Engineering Science and Ocean Engineering, National Taiwan University, Taipei, Taiwan, in 2020. He is currently pursuing the Ph.D. degree in electrical and computer engineering with Rice University, Houston, TX, USA.

ZONG-HAN CAI received the B.S. degree in mechanical and electromechanical engineering from National Sun Yat-sen University, Kaohsiung, in 2020. He is currently pursuing the M.S. degree in engineering science and ocean engineering with National Taiwan University, Taipei, Taiwan.

HUNG-HSUN CHEN received the B.S. degree in systems engineering and naval architecture from National Taiwan Ocean University, Keelung, in 2017, and the M.S. degree in engineering science and ocean engineering from National Taiwan University, Taipei, in 2019. He is currently an Equipment Engineer at Taiwan Semiconductor Manufacturing Company Ltd., Tainan, Taiwan.

CHENG-HSIEN CHUNG received the B.S. and M.S. degrees in naval architecture and ocean engineering from National Taiwan University, Taipei, 1993 and 1995, respectively, and the Ph.D. degree in engineering science and ocean engineering from National Taiwan University, Taipei, in 2003. He is currently the Chief of the Project Management Office, Ship and Ocean Industries Research and Development Center (SOIC), Taipei, Taiwan.

I-CHUNG CHENG received the B.S. degree in mechanical engineering and the M.S. degree in materials science and engineering from National Taiwan University, in 2005 and 2007, respectively, and the Ph.D. degree in materials science from the University of Southern California, in 2013. From 2013 to 2015, he was a Postdoctoral Fellow at the Hodge Research Laboratory, Department of Aerospace and Mechanical Engineering, University of Southern California, where he was involved in the mechanical behavior of structural amorphous metals and single crystals. In 2017, he joined National Taiwan University, where he is currently an Assistant Professor with the Department of Mechanical Engineering. His research interests include nanoporous metal films, surface modification, and electrocatalysts.

YUEH-LIEN LEE (Member, IEEE) received the B.S. and M.S. degrees in mechanical engineering from National Central University, Taoyuan, in 2004 and 2005, respectively, and the Ph.D. degree in materials science and engineering from National Taiwan University, Taipei, in 2011. From 2011 to 2014, he was a Postdoctoral Fellow at the Fontana Corrosion Center, Department of Materials Science and Engineering, The Ohio State University, Columbus, OH, USA, where he was involved in electrochemistry of corrosion, corrosion prediction, and corrosion protection. In 2014, he joined National Taiwan University, where he is currently an Associate Professor with the Department of Engineering Science and Ocean Engineering. His research interests include corrosion monitoring, surface modification, and corrosion-resistant coatings.